RSC Advances

PAPER

View Article Online
View Journal | View Issue

Cite this: *RSC Adv.*, 2017, **7**, 9123

Preparation and study of a mesoporous silica-coated Fe_3O_4 photothermal nanoprobe

N. Q. Yin,* P. Wu, T. H. Yang and M. Wang

A mesoporous silica-coated Fe_3O_4 nanoprobe exhibiting a high photothermal conversion efficiency was synthesized by a facile and green approach. The silica shell with a mesoporous structure was obtained using tetraethyl orthosilicate as the silica source, cationic surfactant cetyltrimethylammonium bromide as the template, and 1,3,5-triisopropylbenzene as a pore swelling agent. The morphology and magnetic properties of the resultant nanoprobe were characterized *via* TEM, XRD and vibrating sample magnetometry (VSM). The nanoprobe, with a well-defined core–shell nanostructure, exhibited strong superparamagnetism at room temperature. Moreover, after cancer cells were cultured with the nanoprobe solution and irradiated for several minutes by laser, the cancer cells were effectively destroyed, demonstrating that this nanoprobe is a good candidate for treating cancer.

Received 19th December 2016
Accepted 18th January 2017

DOI: 10.1039/c6ra28413b

rsc.li/rsc-advances

1 Introduction

The application of nanomaterials in the biomedical area, also named as nanomedicine, has gained much attention due to their fascinating photoelectric and magnetic properties.[1–6] An important area of nanomedicine is concerned with the development of photothermal nanoprobes.[7–9] Nanoprobes utilize the intense absorption characteristics of nanomaterials, converting the incident photon into heat energy very efficiently. Moreover, the local heat energy greatly increases the temperature in the area around the nanomaterial, which can destroy the targeted cancer cells. Compared with traditional cancer treatments, such as radiotherapy, chemotherapy and surgery, photothermal therapy is a non-invasive and targeted therapeutic intervention for specific biological tissues. As an ideal photothermal agent, a nanomaterial should meet several requirements: (i) low cytotoxicity, (ii) good dispersibility in the biological environment, (iii) high thermostability and photostability, (iv) near-infrared (NIR) absorption in the range of 600–900 nm to minimize absorption by the surrounding healthy tissues and thereby avoiding damage to these tissues (v) low cost, and (vi) being accessible by a simple preparation method.

With the rapid development of nanoscience and biotechnology, several nanomaterials have been synthesized and studied. In the search of the ideal photothermal nanoprobe, a number of materials have been extensively explored including noble metal nanoparticles (gold nanocage,[10–12] gold nanostar[13–15] and Pd nanoflower[16–18]), carbon-based nanoparticles (carbon nanotubes[19,20] and graphene[21,22]), semiconductor nanoparticles (copper sulfide[23]), and organic nanomaterials.[24] However, the nature of these photothermal nanoprobes limited their wide application in the area of photothermal therapy. For example, noble metal nanoparticles,[11,16] which were used as photothermal nanoprobes based on their local surface plasmon resonance, have a high preparation cost and low thermostability under long-term laser irradiation. Carbon-based nanomaterials,[19,22] after being mainlined to the target body tissues, can give rise to serious pulmonary inflammation and oxidative stress. Semiconductor nanoparticles and organic nanomaterials have low photothermal conversion efficiencies and exhibit certain biological toxicity. Considering the various unwanted adverse effects of these nanoparticles, it is highly urgent to develop a novel photothermal nanoprobe with low cytotoxicity and high photothermal conversion efficiency.

As an important biomedical nanomaterial, iron oxide (Fe_3O_4) nanoparticles receive much attention due to its unique features, namely low cytotoxicity, excellent biocompatibility, fast magnetic response and controllable sizes.[25–27] Recently, the Food and Drug Administration (FDA) has reported that Fe_3O_4 nanoparticles have been approved as a contrast agent for T2-weighted MRI. Iron oxide has been extensively explored in numerous biomedical areas,[26,27] such as targeted drug delivery, magnetic heat treatment and MR imaging. In addition, iron oxide can be used as a photothermal nanoprobe against cancer cells,[28–30] as reported by several research groups. However, conventional Fe_3O_4 nanoparticles are usually synthesized *via* a hydrothermal method without any modification, which often leads to aggregation and precipitation of the particles. In order to solve this problem, surface modifications and surface coating are common strategies to improve the stability of Fe_3O_4 nanoparticles. Mesoporous silica is a common material for surface passivation.[31–33] As it is known, mesoporous silica can be easily coated on the surfaces of

School of Physics and Electrical Information, Shangqiu Normal University, Shangqiu 476000, Henan, People's Republic of China. E-mail: yinnq@foxmail.com; Tel: +86 370 2585825

nanoparticles and prevent the aggregation phenomenon in biomedical applications. Another advantage is that mesoporous silica is terminated by silanol groups, which can be easily modified by alkoxysilane groups covalently bonded to the silica surface. Moreover, due to its attractive physicochemical properties, such as high porosity and large specific surface area, mesoporous silica has attracted great attention in numerous biomedical areas ranging from drug delivery to catalysis.

Inspired by these facts, in this study, we report the synthesis of novel mesoporous silica-coated Fe_3O_4 nanoparticles, and study their use as a photothermal nanoprobe against cancer cells. According to data obtained *via* X-ray diffraction and transmission electron microscopy, the mesoporous silica-coated Fe_3O_4 nanoparticles have an excellent structure and morphology. The photothermal conversion efficiency test indicated that the silica-coated Fe_3O_4 nanoprobe has a good light absorption ability. When cancer cells are cultured with the photothermal nanoprobe and irradiated for several minutes, numerous cancer cells are killed, but no effect is observed on normal cells. These results demonstrate that these silica-coated Fe_3O_4 nanoparticles are an excellent photothermal nanoprobe for destroying cancer cells.

2 Experimental

2.1 Materials

Ferrous sulfate ($FeSO_4 \cdot 7H_2O$, 99%, AR), ferric chloride ($FeCl_3 \cdot 6H_2O$, 97%, AR), absolute ethanol (99.7%, AR), ammonia (28% NH_3, AR), ethylene glycol (EG, 99.5%, AR), oleic acid (98%, AR), tetraethyl orthosilicate (TEOS, 28.4% SiO_2, AR), ammonium nitrate (99.5%, AR), 99.5% folic acid (FA, 98%, AR) and hydrochloric acid (HCl, 36%, AR) were obtained from Sinopharm Chemical Reagent Co., Ltd, China. The resistivity of the deionized water was 18.25 ($M\Omega\ cm^{-1}$). 1,3,5-Trimethyl-benzene (TMB, 99%, AR), cetylmethyl ammonium bromide (CTAB, AR), and 3-aminopropyltrimethoxysilane (APS, 99%, AR) were purchased from Sigma-Aldrich. The breast cancer cell line (SK-BR-3) was provided by the First Affiliated Hospital of the Anhui Medical University.

2.2 Preparation of oleic acid-stabilized Fe_3O_4 nanoparticles

A revised chemical coprecipitation method and modified procedure were used to prepare oleic acid-stabilized Fe_3O_4 nanoparticles. Briefly, the procedure is as follows: (i) a 50 mL aqueous mixture solution composed of 0.05 mol $FeCl_3 \cdot 6H_2O$ and 0.025 mol $FeSO_4 \cdot 7H_2O$ was prepared in a 150 mL three-necked flask, and the mixture was bubbled three times with nitrogen under continuous mechanical agitation. (ii) The pH of the mixture was adjusted to 9.8 with ammonia solution. (iii) Temperature was raised to 80 °C and mixture was allowed to react for 30 min in oil bath with mechanical stirring under N_2 atmosphere. Then, 2.2 mL of oleic acid was quickly added and the resulting mixture was allowed to react for 3 hours. (iv) The product was magnetically separated and washed with deionized water three times. Finally, the oleic acid-stabilized Fe_3O_4 nanoparticles were dispersed in 50 mL of chloroform for further characterization and use.

2.3 Synthesis of mesoporous silica-coated Fe_3O_4 nanoparticle

Method one. In a typical preparation procedure, 1 mL of a prepared Fe_3O_4 nanoparticle solution was mixed with 30 mL of a 0.6 M CTAB solution. Then, the mixture was sonicated at 70 °C for one hour, forming an oil-in-water microemulsion. The residual chloroform was evaporated to give a transparent water-soluble dispersion driven by the van der Waals interactions between the oleic acid molecules and the hydrocarbon chains of CTAB. A solution composed of 10 mL of EG, 0.7 mL of aqueous ammonia solution and 30 mL of deionized water was added to the CTAB/Fe_3O_4 solution, and the final mixture was aged at 70 °C for 10 min under continuous vigorous mechanical stirring. Subsequently, a TEOS solution was dropwise added to the mixture at a speed of 30 μL per hour. In order to form mesoporous silica-coated Fe_3O_4 nanoparticles with large silica pores, a certain amount of TMB was added to the reaction mixture and allowed to react for 2 hours prior to the addition of TEOS. As an expanding agent, the dosage of TMB can tune the size of the silica pores. After vigorous stirring at 70 °C for 6 h, the mixture was washed with deionized water several times and dispersed in absolute ethanol. Finally, the obtained nanoparticles were dispersed in a 40 mL ethanol solution containing 2 mmol of ammonium nitrate, and the mixture was stirred at 60 °C for 30 min. The last procedure was repeated at least three times and the obtained product was dispersed in 30 mL of absolute ethanol for further use.

Method two. This is a new method to form mesoporous silica-coated Fe_3O_4 nanoparticles with a large Fe_3O_4 core and large silica pores. The main preparation procedure is the same as the one described above, with the difference that after the solution consisting of EG, aqueous ammonia solution and deionized water was added into the CTAB/Fe_3O_4 mixture, mechanical stirring is maintained at low speed. Besides, the thickness of the silica shell and the size of the silica pore can be controlled with the amount of TEOS and TMB.

2.4 Synthesis of the mesoporous silica-coated Fe_3O_4 photothermal nanoprobe

The mesoporous silica-coated Fe_3O_4 nanoparticles with a large Fe_3O_4 core were used to prepare the photothermal nanoprobe. The nanoparticles were modified with an APS solution: an APS ethanolic solution (0.5 mL of APS in 100 mL of absolute ethanol) was mixed with the mesoporous silica-coated Fe_3O_4 nanoparticles under vigorous mechanical stirring. After reacting for 12 hours at 60 °C, the product was washed and redissolved in 10 mL of deionized water. Then, 0.1 mL of folic acid was slowly added to the mixture solution. After mechanical stirring for 6 hours, the folic acid-modified photothermal nanoprobe was centrifuged and dispersed in 10 mL of deionized water.

2.5 Cytotoxicity

The cytotoxicity of the mesoporous silica-coated Fe_3O_4 nanoprobe was evaluated using the MTT assay in the SK-BR-3 breast cancer cell line. Various solutions of the nanoprobe with

different concentrations, ranging from 0 to 2 mg mL^{-1}, were prepared by mixing the nanoprobe with the required amount of water. After cells were treated with the nanoprobe solution for 24 h, cell viability was assessed by the MTT method and expressed as the percentage of the surviving cells. All data presented are the mean values of five independent measurements.

2.6 Photothermal conversion experiment for mesoporous silica-coated Fe_3O_4 nanoprobe *in vitro*

SK-BR-3 cancer cells were used for the photothermal *in vitro* experiment with the nanoprobe. Cancer cells were harvested from the cell culture plate, seeded onto a 96-well plate at a density of 5×10^3 cells per well and incubated at 37 °C in 5% CO_2 (v/v) for 24 hours. Then, the cancer cells were washed three times with the cell growth solution. A mixture of 1.9 mL of fresh DMEM (supplemented with 10% FBS) and 0.1 mL of photothermal nanoprobe solution were added to the culture plate and cultured for 4 hours at 37 °C in 5% CO_2 (v/v). As the culture plate was being washed with PBS solution, the cancer cells were exposed to NIR laser light of an intensity tuned at 1 W cm^{-2}. After being irradiated for 10 minutes, cancer cells were stained and the viability was examined under a fluorescence microscope.

2.7 Characterization

The crystal structure was determined *via* X-ray diffraction, conducted under Cu Kα (0.154 nm) radiation. The microstructure of the nanoparticles was determined using a JEM-1400 transmission electron microscope at an acceleration voltage of 120 kV. The magnetic hysteresis loop was measured by vibrating sample magnetometry (VSM; Quantum Design) at room temperature. A temperature detector was used for real-time monitoring of the temperature changes in the nanoprobe.

3 Results and discussion

The logical synthesis of the mesoporous silica-coated Fe_3O_4 nanoprobe and its usage in photothermal therapy against cancer cells is illustrated in Fig. 1. A traditional hydrothermal method was used to prepare the Fe_3O_4 nanoparticles, which were modified and stabilized using oleic acid. Then, the Fe_3O_4 nanoparticles were coated with a silica shell *via* the Stöber method. The silica shell was etched into a mesoporous structure using CTAB and TMA as the swelling agents. As the mesoporous silica-coated Fe_3O_4 was modified using FA, relative photothermal tests were carried out on the photothermal nanoprobe.

It is well known that for a nanoparticle, a good dispersibility in solution is critical for its further synthesis and use. Thus, in order to improve the dispersibility of the Fe_3O_4 nanoparticles in solution, a modified hydrothermal method was employed to synthesize oleic acid-stabilized Fe_3O_4 nanoparticles, which can be evenly dispersed in chloroform solution. Fig. 2a shows the TEM image of oleic acid-stabilized Fe_3O_4 nanoparticles, with an average particle diameter of 12 nm and a narrow size distribution, according to particle size statistics. By the addition of CTAB amphiphilic molecules, a phase transfer from oleic phase to aqueous phase occurred on the oleic acid-stabilized Fe_3O_4 nanoparticles. As is known, pure Fe_3O_4 nanoparticles aggregate easily and form large clusters, and thus lose their special magnetic properties.[34,35] Surface passivation is a useful method to improve the stability of Fe_3O_4 nanoparticles. A silica shell was coated onto the surface of Fe_3O_4 nanoparticles *via* a modified Stöber method.[31,32] The as-prepared mesoporous silica-coated Fe_3O_4 nanoparticles have a good dispersibility, as revealed from the TEM images (Fig. 2b and c). Due to its excellent drug loading capacity, mesoporous silica was introduced into the silica shell instead of conventional silica, using TEOS as the mesoporous silica source and TMB as the pore swelling agent. For photothermal nanoparticles, photothermal conversion is dominated by the Fe_3O_4 nanoparticles, and therefore two types of mesoporous silica-coated Fe_3O_4 nanoparticles were prepared through adjusting the speed of the mechanical stirring and the amount of TEOS during silica coating. Mesoporous silica-coated Fe_3O_4 nanoparticles with a small Fe_3O_4 core (Fig. 2b) were obtained using high stirring speed and a large amount of TEOS, which maintained the uniform dispersion of Fe_3O_4 nanoparticles throughout the entire process. By contrast, mesoporous silica-coated Fe_3O_4 nanoparticles with a large Fe_3O_4 core (Fig. 2c) were produced with low stirring speed due to the anisotropic dipolar attraction of adjacent Fe_3O_4 nanoparticles. Moreover, as shown in Fig. 2c, the pore size of the silica shell was enlarged through the addition of large amounts of TMB,

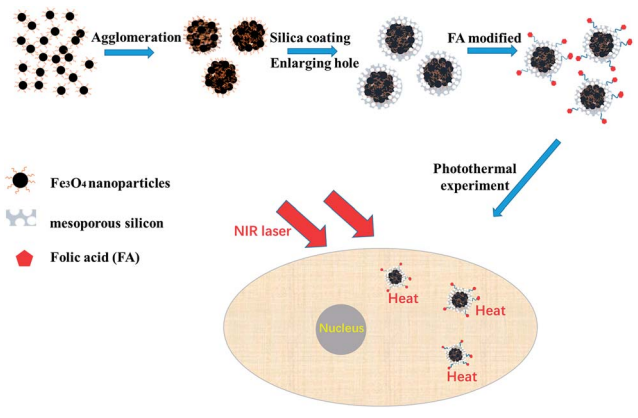

Fig. 1 Schematic of the preparation of the mesoporous silica-coated Fe_3O_4 nanoprobe and its usage in photothermal therapy.

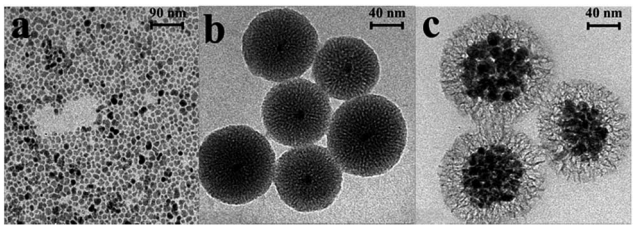

Fig. 2 TEM images of (a) oleic acid-stabilized Fe_3O_4 nanoparticles, (b) mesoporous silica-coated Fe_3O_4 nanoparticles with a small Fe_3O_4 core and (c) mesoporous silica-coated Fe_3O_4 nanoparticles with a large Fe_3O_4 core and large silica pores.

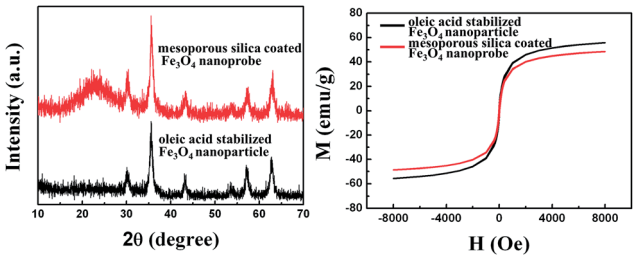

Fig. 3 (a) Powder X-ray diffraction (XRD) patterns of oleic acid-stabilized Fe_3O_4 nanoparticles and the mesoporous silica-coated Fe_3O_4 nanoprobe, (b) magnetic curves of oleic acid-stabilized Fe_3O_4 nanoparticles and the mesoporous silica-coated Fe_3O_4 nanoprobe.

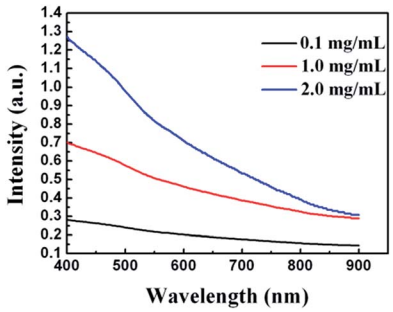

Fig. 4 Absorption spectra of the mesoporous silica-coated Fe_3O_4 nanoprobe at different concentrations (0.1 mg mL^{-1}, 1.0 mg mL^{-1} and 2.0 mg mL^{-1}).

which is beneficial for biomolecule- and drug-loading. In the mesoporous silica-coated Fe_3O_4 nanoparticles obtained by this synthetic process, based on the dosage of every reagent and considering the loss of sample, the mass ratio of Fe_3O_4 and mesoporous silica was determined to be approximately 7.1 : 1 (Fig. 2c).

As shown in Fig. 3a, the X-ray diffraction pattern exhibited well-defined diffraction peaks for both oleic acid-stabilized and mesoporous silica-coated Fe_3O_4 nanoparticles. The XRD pattern (in black) of the oleic acid-stabilized Fe_3O_4 nanoparticles is consistent with that of the standard Fe_3O_4 nanoparticles (JCPDS 19-0629), confirming the formation of Fe_3O_4 nanoparticles. According to the Debye–Scherer formula, the size of the Fe_3O_4 nanoparticle was calculated to be around 13 nm. As seen in Fig. 3a, the XRD pattern of the mesoporous silica-coated Fe_3O_4 nanoparticles (in red) displays the same diffraction peaks as the XRD pattern of oleic acid-stabilized Fe_3O_4 nanoparticles. It was thus demonstrated that Fe_3O_4 nanoparticles were successfully coated by mesoporous silica and that the crystal structure of Fe_3O_4 was not affected during the mesoporous silica coating step. Furthermore, in the XRD pattern, a characteristic peak at around 20° indicated the amorphous nature of the mesoporous silica. From the magnetic curves, recorded at room temperature, it was found that both oleic acid-stabilized and mesoporous silica-coated Fe_3O_4 nanoparticles were superparamagnetic, with magnetization saturation values of 55.7 and 48.6 emu g^{-1}, respectively (Fig. 3b). This result indicated that the mesoporous silica-coated Fe_3O_4 nanoparticles are an excellent magnetic carrier, which can be used in targeted transport, magnetic separation and other applications.

Recently, it was reported that Fe_3O_4 nanoparticles could be used as a photothermal nanoprobe due to their low toxicity, excellent biocompatibility and broad absorption.[28–30] Fig. 4 shows the absorption spectra of the mesoporous silica-coated Fe_3O_4 nanoprobe at different concentrations. The mesoporous silica-coated Fe_3O_4 nanoprobe exhibits a broad absorption within the visible to near-infrared range, which is suitable for a multi-wavelength absorber. Moreover, the absorption intensity of the nanoprobe solution was enhanced with the increasement of the concentration, which was accorded with the general absorption regularity.

As is known, biological tissues have less absorption in the near-infrared (NIR) region,[36,37] such that NIR light can only penetrate a few centimeters in biological tissues. Therefore, NIR light has been often used as the laser light source in experiments of photothermal therapy. In order to evaluate the photothermal effect with NIR laser irradiation, three solutions of mesoporous silica-coated Fe_3O_4 nanoparticles with different concentrations (10 mg mL^{-1}, 1 mg mL^{-1} and 0.1 g mL^{-1}) and a pure water sample as the control, were measured. As shown in Fig. 5, the temperature of all the samples increased with the irradiation time and reached a saturation temperature at 600 seconds. Significantly, the temperature increased more rapidly in the samples with higher concentrations. The final temperature of the three samples (10 mg mL^{-1}, 1 mg mL^{-1} and 0.1 mg mL^{-1}) was enhanced by 28.3 °C, 24.3 °C, and 11.1 °C, respectively. In the data reported, each temperature value was the average of three separate measurements. The enhanced temperature for the sample with 1 mg mL^{-1} concentration is high enough to destroy the targeted cancer cells or tissues. By contrast, the temperature of the control sample (pure water) increased by only 4 °C after constant irradiation under similar conditions. The small temperature increase of the control sample has no adverse

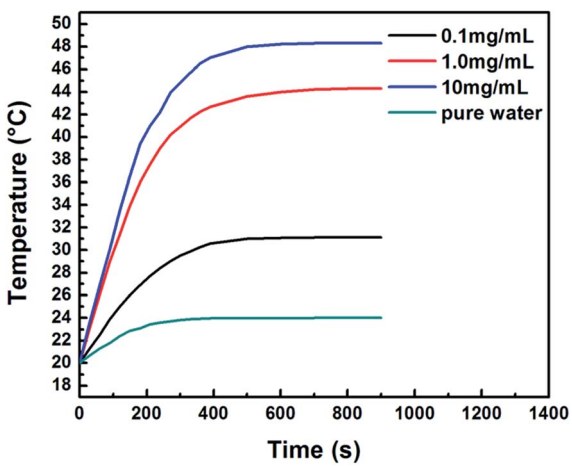

Fig. 5 Increase in the temperature of the aqueous dispersion of the mesoporous silica-coated Fe_3O_4 nanoprobe at different concentrations as a function of the irradiation time. All the samples were irradiated with a 808 nm laser at 1 W cm^{-2} for 15 min.

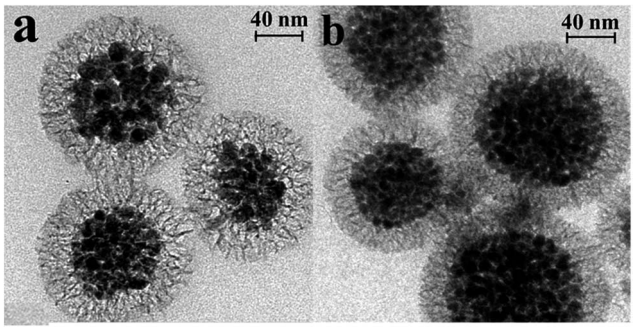

Fig. 6 TEM images of (a) mesoporous silica-coated Fe_3O_4 nanoparticles before laser irradiation, (b) mesoporous silica-coated Fe_3O_4 nanoparticles after laser irradiation at a power density of 1 W cm^{-2} for 15 min.

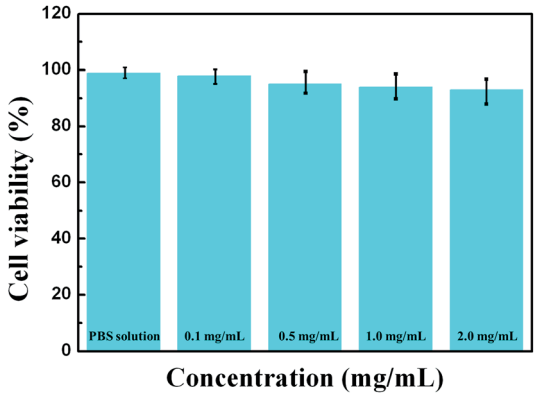

Fig. 7 Cell viability assay of the SK-BR-3 cell line after incubation with the mesoporous silica-coated Fe_3O_4 nanoprobe.

effects on the normal cells and tissues, as the final temperature is still below the threshold temperature (42 °C) that causes biomacromolecules (such as proteins) to denature. It is known that a good photothermal nanoprobe should have an excellent thermostability, otherwise the nanoprobe will lose its photothermal conversion ability and will affect the normal body tissues. The effect of laser irradiation on the morphology of the mesoporous silica-coated Fe_3O_4 nanoprobe was investigated *via* TEM, as shown in Fig. 6. Fig. 6a and b display the TEM images of the nanoprobe before and after laser irradiation, respectively, at a power density of 1 W cm^{-2} for 15 min. From the TEM images, it can be seen that the laser irradiation has little effect on the morphology of the nanoprobe, which demonstrates that the nanoprobe has excellent thermostability and can be used as a photothermal nanoprobe.

In order to confirm the photothermal conversion ability of mesoporous silica-coated Fe_3O_4 nanoparticles *in vitro*, the surface of the nanoparticles was modified with PA to increase the biocompatibility by electrostatic interactions. In the modifying progress, the mesoporous silica-coated Fe_3O_4 nanoparticles were treated with APS, introducing $-NH_2$ groups on the surface of the nanoparticles. Subsequently, the $-NH_2$ groups of APS were used to form amide bonds with the –COOH groups of PA.

It was necessary to measure the cytotoxicity of the mesoporous silica-coated Fe_3O_4 nanoprobe before using it for photothermal therapy. Thus, the cell viability of the nanoprobe was evaluated using the MTT assay. SK-BR-3 breast cancer cells were chosen as the model cell line. As seen from Fig. 7, after the SK-BR-3 cancer cells were treated with the nanoprobe for 24 h at concentrations ranging from 0 to 2 mg mL^{-1}, cell viability was over 90% for all concentrations, and the nanoprobe did not exhibit any evident cytotoxicity against the cells. These results indicated that the mesoporous silica-coated Fe_3O_4 nanoprobe has a good biocompatibility and is suitable for biological research.

Inspired by the excellent photothermal effect of the mesoporous silica-coated Fe_3O_4 nanoprobe, we used the mesoporous silica-coated Fe_3O_4 nanoprobe with a concentration of 1 mg mL^{-1} to study the photothermal ablation ability towards cancer cells. The control group was treated with PBS solution. To visually examine the viability of cancer cells, a dual-staining kit containing metanil yellow and ethidium bromide was used to reveal the state of the cancer cells. Apparently, after the cancer cells were treated with the nanoprobe solution and irradiated for 10 min with a 808 nm laser at a power density of 1.0 W cm^{-2}, the viability of cancer cells markedly decreased (Fig. 8a). In sharp contrast, the control group after irradiation at the same power density and during the same time showed no changes (Fig. 8b), indicating the negligible phototoxicity of our irradiation conditions.

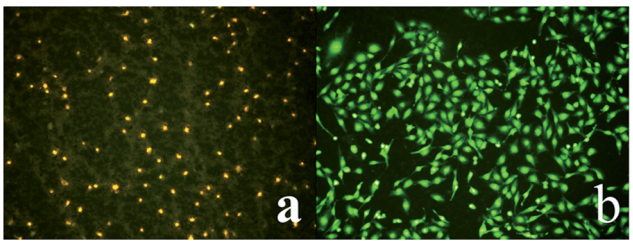

Fig. 8 Treatment of SK-BR-3 breast cancer cells with (a) the mesoporous silica-coated Fe_3O_4 nanoprobe, and (b) PBS solution. All samples were irradiated with a 808 nm laser at 1 W cm^{-2} for 10 min.

4 Conclusion

In summary, we synthesized a mesoporous silica-coated Fe_3O_4 nanoprobe through a modified Stöber method, effectively regulating the sizes of the Fe_3O_4 core and silica pores for the first time. The obtained nanoprobe possessed well-defined structural features, high cytocompatibility, low cytotoxicity and strong NIR absorption. These excellent properties allow its application in photothermal therapy towards cancer cells. Furthermore, the nanoprobe could generate a large amount of local heat under NIR irradiation and destroy the cancer cells due to its strong photothermal ablation ability. These results demonstrate the potential for using mesoporous silica-coated Fe_3O_4 nanoprobes for applications in cancer therapy.

Acknowledgements

This study was supported by the National Natural Science Foundation of China (No. 11647019) and the Henan Provincial Educational Committee Program (No. 17B430004).

Notes and references

1 L. Cheng, K. Yang, Q. Chen and Z. Liu, Organic stealth nanoparticles for highly effective *in vivo* near-infrared photothermal therapy of cancer, *ACS Nano*, 2012, **6**, 5605–5613.

2 Y. Wang, K. Y. Wang, R. Zhang, X. G. Liu, X. Y. Yan, J. X. Wang, E. Wagner and R. Q. Huang, Synthesis of core-shell graphitic carbon@silica nanospheres with dual-ordered mesopores for cancer-targeted photothermochemotherapy, *ACS Nano*, 2014, **8**, 7870–7879.

3 Y. C. Chen, W. T. Chiu, J. C. Chen, C. S. Chang, L. H. C. Wang, H. P. Lin and H. C. Chang, The photothermal effect of silica-carbon hollow sphere-concanavalin A on liver cancer cells, *J. Mater. Chem. B*, 2015, **3**, 2447–2454.

4 A. H. Lu, T. Sun, W. C. Li, Q. Sun, F. Han, D. H. Liu and Y. Guo, Synthesis of discrete and dispersible hollow carbon nanospheres with high uniformity by using confined nanospace pyrolysis, *Angew. Chem., Int. Ed.*, 2011, **50**, 11765–11768.

5 G. X. Wang, N. N. Cao and Y. Y. Wang, Characteristics and corrosion studies of zinc–manganese phosphate coatings on magnesium–lithium alloy, *RSC Adv.*, 2014, **4**, 59772–59778.

6 X. H. Huang, S. Neretina and M. A. El-Sayed, Gold nanorods: From synthesis and properties to biological and biomedical applications, *Adv. Mater.*, 2009, **21**, 4880–4910.

7 F. Chen, H. Hong, S. Goel, S. A. Graves, H. Orbay, E. B. Ehlerding, S. X. Shi, C. P. Theuer, R. J. Nickles and W. B. Cai, *In vivo* tumor vasculature targeting of CuS@MSN based theranostic nanomedicine, *ACS Nano*, 2015, **9**, 3926–3934.

8 W. P. Li, P. Y. Liao, C. H. Su and C. S. Yeh, Formation of oligonucleotide-gated silica shell-coated Fe_3O_4–Au core-shell nanotri soctahedra for magnetically targeted and near-infrared light-responsive theranostic platform, *J. Am. Chem. Soc.*, 2014, **136**, 10062–10075.

9 S. S. Lucky, N. M. Idris, Z. Q. Li, K. Huang, K. C. Soo and Y. Zhang, Titania coated upconversion nanoparticles for near-infrared light triggered photodynamic therapy, *ACS Nano*, 2015, **9**, 191–205.

10 J. G. Piao, L. M. Wang, F. Gao, Y. Z. You, Y. J. Xiong and L. H. Yang, Erythrocyte membrane is an alternative coating to poly-ethylene glycol for prolonging the circulation lifetime of gold nanocages for photothermal therapy, *ACS Nano*, 2014, **8**, 10414–10425.

11 B. N. Khlebtsov, V. A. Khanadeev, E. V. Panfilova, T. E. Pylaev, O. A. Bibikova, S. A. Staroverov, V. A. Bogatyrev, L. A. Dykman and N. G. Khlebtsov, New types of nanomaterials: powders of gold nanospheres, nanorods, nanostars, and gold–silver nanocages, *Nanotechnol. Russ.*, 2013, **8**, 209–219.

12 J. Y. Chen, C. Glaus, R. Laforest, Q. Zhang, M. X. Yang, M. Gidding, M. J. Welch and Y. N. Xia, Gold nanocages as photothermal transducers for cancer treatment, *Small*, 2010, **6**, 811.

13 B. J. Du, X. X. Gu and W. J. Zhao, Hybrid of gold nanostar and indocyanine green for targeted imaging-guided diagnosis and phototherapy using low-density laser irradiation, *J. Mater. Chem. B*, 2016, **35**, 5842–5849.

14 E. C. Hao, R. Bailey, G. C. Schatz, J. T. Hupp and S. Y. Li, Synthesis and optical properties of "branched" gold nanocrystals, *Nano Lett.*, 2004, **4**, 327–330.

15 L. C. Chen, J. H. Huang, H. M. Chen, T. C. Lai, K. Y. Yang, R. S. Liu, M. Hsiao, C. H. Chen, L. J. Her and D. P. Tsai, Seedless, silver-induced synthesis of star-shaped gold/silver bimetallic nanoparticles as high efficiency photothermal therapy reagent, *J. Mater. Chem.*, 2012, **22**, 2244–2253.

16 Y. Q. Jiang, J. Y. Su and Y. N. Yang, A facile surfactant-free synthesis of Rh flower-like nanostructures constructed from ultrathin nanosheets and their enhanced catalytic properties, *Nano Res.*, 2016, **3**, 849–856.

17 C. Ma, Y. Y. Du, J. T. Feng, X. Z. Cao, J. Yang and D. Q. Li, Fabrication of supported PdAu nanoflower catalyst for partial hydrogenation of acetylene, *J. Catal.*, 2014, **317**, 263–271.

18 Q. Y. Wang, X. Q. Cui and W. M. Guan, A nanoflower shaped gold-palladium alloy on graphene oxide nanosheets with exceptional activity for electrochemical oxidation of ethanol, *Microchim. Acta*, 2013, **181**, 373–380.

19 Y. Meng, S. S. Wang and C. Y. Li, Photothermal combined gene therapy achieved by polyethyleneimine-grafted oxidized mesoporous carbon nanospheres, *Biomaterials*, 2016, **100**, 134–142.

20 G. H. Wang, F. Zhang and R. Tian, Nanotubes-embedded indocyanine green-hyaluronic acid nanoparticles for photoacoustic-imaging-guided phototherapy, *ACS Appl. Mater. Interfaces*, 2016, **8**, 5608–5617.

21 S. Wang, Q. Luo and X. F. Zhang, Magnetic graphene-based nanotheranostic agent for dual-modality mapping guided photothermal therapy in regional lymph nodal metastasis of pancreatic cancer, *Biomaterials*, 2014, **35**, 9473–9483.

22 L. Y. Xu and X. N. Yang, Molecular dynamics simulation of adsorption of pyrene-polyethylene glycol onto graphene, *J. Colloid Interface Sci.*, 2014, **432**, 128–134.

23 J. Mou, P. Li and C. B. Liu, Ultrasmall $Cu_{2-x}S$ nanodots for highly efficient photoacoustic imaging-guided photothermal therapy, *Small*, 2015, **11**, 2275–2283.

24 H. Zhang, L. F. Xiong and X. J. Liao, Controlled-release system of small molecules triggered by the photothermal effect of polypyrrole, *Macromol. Rapid Commun.*, 2016, **37**, 149–154.

25 J. H. Chen, S. Pang and L. L. He, Highly sensitive and selective detection of nitrite ions using Fe_3O_4@SiO_2/Au magnetic nanoparticles by surface-enhanced Raman spectroscopy, *Biosens. Bioelectron.*, 2016, **85**, 726–733.

26 J. N. Zhang, K. X. Wang and Q. Xu, Beyond yolk-shell nanoparticles: Fe_3O_4@Fe_3C core@shell nanoparticles as

yolks and carbon nanospindles as shells for efficient lithium ion storage, *ACS Nano*, 2015, **9**, 3369–3376.

27 M. Ye, Z. W. Wei and F. Hu, Fast assembling microarrays of superparamagnetic Fe_3O_4@Au nanoparticle clusters as reproducible substrates for surface-enhanced Raman scattering, *Nanoscale*, 2015, **7**, 13427–13437.

28 Y. Li, H. T. T. Duong, S. Laurent, A. MacMillan, R. M. Whan, L. V. Elst, R. N. Muller, J. Hu, A. Lowe, C. Boyer and T. P. Davis, Nanoparticles based on star polymersas the ranostic vectors: endosomal-trigge red drug release combined with MRI sensitivity, *Adv. Healthcare Mater.*, 2015, **4**, 148–156.

29 L. S. Lin, Z. X. Cong, J. B. Cao, K. M. Ke, Q. L. Peng, J. Gao, H. H. Yang, G. Liu and X. Chen, Multifunctional Fe_3O_4@polydopamine core–shell nanocomposites for intracellular mRNA detection and imaging-guided photothermal therapy, *ACS Nano*, 2014, **8**, 3876–3883.

30 J. C. Li, Y. Hu, J. Yang, P. Wei, W. J. Sun, M. W. Shen, G. X. Zhang and X. Y. Shi, Hyaluronic acid-modified Fe_3O_4@Au core/shell nanostars for multimodal imaging and photothermal therapy of tumors, *Biomaterials*, 2015, **38**, 10–21.

31 J. P. Lai, B. R. Shah and Y. X. Zhang, Real-time monitoring of ATP-responsive drug release using mesoporous-silica-coated multicolor upconversion nanoparticles, *ACS Nano*, 2015, **9**, 5234–5245.

32 M. Benezra, E. Phillips and M. Overholtzer, Ultrasmall integrin-targeted silica nanoparticles modulate signaling events and cellular processes in a concentration-dependent manner, *Small*, 2015, **11**, 1721–1732.

33 D. Li, B. Mathew and C. B. Mao, Biotemplated synthesis of hollow double-layered core/shell titania/silica nanotubes under ambient conditions, *Small*, 2012, **8**, 3691–3697.

34 Y. M. Huh, *In vivo* magnetic resonance detection of cancer by using multifunctional magnetic nanocrystals, *J. Am. Chem. Soc.*, 2005, **127**, 12387–12391.

35 C. Li, Gold-coated Fe_3O_4 nanoroses with five unique functions for cancer cell targeting, imaging, and therapy, *Adv. Funct. Mater.*, 2013, **24**, 1772–1780.

36 W. R. Chen, R. L. Adams, R. Carubelli and R. E. Nordquist, Laser-photosensitizer assisted immunotherapy: a novel modality for cancer treatment, *Cancer Lett.*, 1997, **115**, 25–30.

37 W. R. Chen, R. L. Adams, A. K. Higgins, K. E. Bartels and R. E. Nordquist, Photothermal effects on murine mammary tumors using indocyanine green and an 808 nm diode laser: an *in vivo* efficacy study, *Cancer Lett.*, 1996, **98**, 169–173.